

GEOSPHERE, v. 14, no. 4,

<https://doi.org/10.1130/GES01558.1>

7 figures; 1 set of supplemental files

CORRESPONDENCE: rps1@williams.edu

CITATION: Scudder, R.P., Murray, R.W., Kutterolf, S., Schindlbeck, J.C., Underwood, M.B., and Wang, K.-L., 2018, Sedimentary inputs to the Nankai subduction zone: The importance of dispersed ash: *Geosphere*, v. 14, no. 4, <https://doi.org/10.1130/GES01558.1>.

Science Editor: Shanaka de Silva
Guest Associate Editor: Robert Stern

Received 15 May 2017
Revision received 16 February 2018
Accepted 30 April 2018



This paper is published under the terms of the CC-BY-NC license.

© 2018 The Authors

Sedimentary inputs to the Nankai subduction zone: The importance of dispersed ash

Rachel P. Scudder^{1,*†}, Richard W. Murray^{1,*}, Steffen Kutterolf^{2,*}, Julie C. Schindlbeck^{2,*}, Michael B. Underwood^{3,*}, and Kuo-Lung Wang^{4,*}

¹Department of Earth and Environment, Boston University, 685 Commonwealth Avenue, Boston, Massachusetts 02215, USA

²Research Center for Marine Geosciences (GEOMAR) Helmholtz Centre for Ocean Research Kiel, Wischhofstraße 1-3, Kiel 24148, Germany

³Department of Earth and Environmental Science, New Mexico Institute of Mining and Technology, 801 Leroy Place, Socorro, New Mexico 87801, USA

⁴Institute of Earth Sciences, Academia Sinica, Taipei 11529, Taiwan

ABSTRACT

We examine the importance of dispersed volcanic ash as a critical component of the aluminosilicate sediment entering the Nankai Trough, located south of Japan's island of Honshu, via the subducting Philippine Sea plate. Multivariate statistical analyses of an extensive major, trace, and rare earth element data set from bulk sediment and discrete ash layers at Integrated Ocean Drilling Program (IODP) Sites C0011 and C0012 quantitatively determine the abundance and accumulation of multiple aluminosilicate inputs to the Nankai subduction zone. We identify the eolian input of continental material to both sites, and we further find that there are an additional three ash sources from Kyushu and Honshu, Japan and other regions. Some of these ash sources may themselves represent mixtures of ash inputs, although the final compositions appear statistically distinct. The dispersed ash comprises 38 ± 7 weight percent (wt%) of the bulk sediment at Site C0011, and 34 ± 4 wt% at Site C0012. When considering the entire sediment thickness at Site C0011, the dispersed ash component supplies 38000 ± 7000 g/cm² of material to the Nankai subduction system, whereas Site C0012 supplies 20000 ± 3000 g/cm². These values are enormous compared to the ~ 2500 g/cm² (C0011) and ~ 1200 g/cm² (C0012) of ash in the discrete ash layers. Therefore, the mass of volcanic ash and chemically equivalent alteration products (e.g., smectite) that are dispersed throughout the stratigraphic succession of bulk sediment appears to be up to 15–17 times greater than the mass of discrete ash layers. The composition of the dispersed ash component at Site C0011 appears linked to that of the discrete layers, and the mass accumulation rate for dispersed ash correlates best with discrete ash layer thickness. In contrast, at Site C0012 the mass accumulation rate for dispersed ash correlates better with the number of ash layers. Together, the discrete ash layers, dispersed ash, and clay-mineral assemblages present a complete record of volcanism and erosion

*E-mail addresses: rps1@williams.edu, rickm@bu.edu, skutterolf@geomar.de, julie.schindlbeck@geow.uni-heidelberg.de, UnderwoodM@missouri.edu, kwang@earth.sinica.edu.tw

[†]Current address: Maritime Studies Program, Williams College and Mystic Seaport, 75 Greenmanville Avenue, Mystic, Connecticut 06355, USA

of volcanic sources; and indicate that mass balances and subduction factory budgets should include the mass of dispersed ash for a more accurate assessment of volcanic contributions to large-scale geochemical cycling.

1. INTRODUCTION

Volcanic ash plays an important role for geochemical budgets of “subduction factory” studies (e.g., Plank and Langmuir, 1998; Stern et al., 2006; Plank et al., 2007, and references therein), including the Nankai Trough Seismogenic Zone Experiment (NanTroSEIZE), located south of Japan's island of Honshu. Knowing how much ash is entering subduction zones is important for understanding recycling of arc-derived material, while the ash itself provides an archive of local, regional, and global magmatic evolution. Many studies predominantly focus on discrete ash layers and have linked the thickness and number of ash layers at a variety of locations and timescales with explosive volcanism (Cambray et al., 1993, 1995; Pouclet et al., 1992; Straub, 2003; Kutterolf et al., 2013; Schindlbeck et al., 2015, 2016a, 2016b). Additionally, reconstructions of eruption intensities and atmospheric circulation patterns have been based on the ash in these discrete layers, both at sea and on land (e.g., Ninkovich et al., 1978; Machida, 1999, 2002; Carey and Sigurdsson, 2000; Rose et al., 2003; Kutterolf et al., 2008a, 2008b). The typical products of ash alteration (e.g., smectite group clay minerals) are also important for modulating the frictional properties of mudstones (e.g., Kopf and Brown, 2003; Ikari et al., 2011) and the fluids released by dehydration reactions (e.g., Saffer et al., 2008; Saffer and McKiernan, 2009).

Of additional interest is the distribution of so called “dispersed ash” that is mixed throughout the bulk sediment rather than occurring in discrete layers. Although the term “ash” normally classifies the grain size of explosive volcanic products (juvenile matter and lithic fragments) in volcanology ($32 \mu\text{m}$ to $2 \mu\text{m}$, e.g., Fisher and Schmincke, 1984), we here use “ash” as a term of origin, particularly as a product (mostly volcanic glass) from explosive volcanism regardless of grain size. Therefore, we refer to *discrete ash layers* as a volcanic product that has been emplaced instantaneously by ash fall or flow processes that

result in a visible layer of ash in the sediment. We define *dispersed ash* and volcanic-rich sediment as material of various grain sizes (including single μm grains) that is mixed throughout the bulk sediment and is not present therefore in a visible layer.

Historically, dispersed ash is an under-utilized repository of information regarding geochemical budgets and tectonic history (Scudder et al., 2009, 2014, 2016; and references therein), and can result from bioturbation of pre-existing discrete ash layers, the settling of airborne or subaqueous ash through the water column, transport by rivers and currents from terrestrially exposed ash deposits, and other processes (e.g., gravity flows). Specifically, for the north-west Pacific, geochemical and quantitative statistical analysis has identified multiple dispersed ash components that together comprise ~30–35 weight percent (wt%) of the sediment mass entering the Izu-Bonin-Mariana subduction system (Scudder et al., 2009, 2014, 2016). These high values are consistent with smear slide data and petrographic studies showing that dispersed glass shards and pumice can comprise as much as 30–40 wt% of the bulk sediment (Straub and Schmincke, 1998; Peters et al., 2000; Scudder et al., 2009, 2014, 2016). Here we present geochemical records from Integrated Ocean Drilling Program (IODP) Sites C0011 and C0012 (Expeditions 322 and 333) to determine the composition of the multiple aluminosilicate sources, including dispersed ash, that compose the hemipelagic sediment entering the Nankai Trough.

2. SOURCES OF VOLCANIC ASH TO THE NANKAI REGION

A main goal of the Nankai Trough Seismogenic Zone Experiment (NanTroSEIZE) is to sample and monitor the up-dip limit of the seismogenic and tsunamigenic zone of the Nankai Trough (Fig. 1), along which mega-thrust earthquakes are known to occur (Tobin and Kinoshita, 2006). Sites C0011 and C0012 were drilled in order to characterize the pre-subduction inputs to the Nankai subduction zone (Saito et al., 2010; Henry et al., 2012a). They are located ~10 km apart in the Shikoku Basin, Japan, ~100 km southeast of the Kii Peninsula and ~160 km west of the Izu-Bonin Arc on the Kashinosaki Knoll, a prominent bathymetric high—as in its current configuration or as an off-axis volcanic seamount (Ike et al., 2008). The Shikoku Basin originated on the Philippine Sea plate during the early and middle Miocene as a result of seafloor spreading in a back-arc setting relative to the Izu-Bonin subduction system (Kobayashi et al., 1995). Located near the crest of the Kashinosaki Knoll, Site C0012 represents a condensed sediment section compared to Site C0011, which is located on the northwestern flank (Fig. 1).

Ash at Sites C0011 and C0012 is likely from multiple regions and geodynamical settings and may result from air load fall out, sudden primary and secondary volcanic mass flows, and/or incorporation of volcanic matter supplied by ocean currents tapping different on-land and submarine source regions and their reworked sediment supply (Schindlbeck et al., 2013; Kutterolf et al., 2014; Mahony et al., 2016). The Japanese arc system (e.g., Honshu, Kyushu) and the Izu-Bonin Mariana (IBM) arc likely provide volcanic material to the Nankai

region (Fig. S1¹). Additional plate tectonic and eruption histories for these arcs are presented in the Supplementary Material (footnote 1).

3. SEDIMENTOLOGY AND STRATIGRAPHY

At both Sites C0011 and C0012, five major sedimentary lithostratigraphic units were defined (Fig. 2). Shipboard smear slide analyses of the bulk sediment (note, *not* of the ash layers) estimate that volcanic ash constitutes an average of ~25–30 wt% of the bulk sediment through Units I and II, and decreases to ~7–15 wt% in Unit III (Saito et al., 2010; Henry et al., 2012a). In Unit IV, the smear slide values vary from ~1% to ~40%, and average ~11% with an increase in Unit V to ~50% on average. The smear slide estimates differentiate between “volcanic glass” and “volcanic lithics” in the bulk sediment, but they do not yield further compositional information and have wide uncertainties, making specific interpretations based on smear slides correspondingly uncertain as well (Saito et al., 2010; Henry et al., 2012a).

4. SAMPLES AND METHODS

We analyzed the major-, trace-, and rare-earth element bulk chemistry of marine sediment from all five units at both Sites C0011 (67 samples) and C0012 (51 samples) by inductively coupled plasma–emission spectrometry (ICP-ES) and ICP–mass spectrometry (ICP-MS) (Table S1 [see footnote 1]) following the methods of Scudder et al. (2014). During sampling of the bulk “background” sediment we specifically avoided discrete ash layers, volcanoclastic and/or tuffaceous sandstone, and siliciclastic turbidites. Additionally, because our study focuses on aluminosilicate sediment, we include in our data set only samples with <<10 wt% Ca, and thus essentially undetectable CaCO_3 , to avoid biogenic and authigenic carbonate. Regardless, as described further below, because the element menu on which we focus our geochemical statistical approach includes only elements not associated with the carbonate fraction, there are no effects from, for example, carbonate dilution on our outcomes. One bulk sediment sample from Site C0011 (322-C0011B-11R-4, 2–35 cm, at 434.66 meters below seafloor [mbsf]) was not included in the statistical treatments because it was found to be very ash, although it is not part of a visually identifiable discrete ash layer. The exclusion of this sample accounts for differences in the models presented here and those of our preliminary work at these sites (Scudder et al., 2016). The findings presented here, therefore, supersede those of Scudder et al. (2016) for Sites C0011 and C0012.

Ash layers were identified from core photos, visual core descriptions, and shipboard “barrel sheets.” Core quality and recovery are influenced by drilling method (hydraulic piston corer versus rotary core barrel) and therefore the number and thickness of ash layers presented here represents a minimum. A total of 337 ash layers were identified at Site C0011 and 179 at Site C0012 (Mahony et al., 2014), ranging in thickness from a few millimeters to 10s of centimeters.

Supplemental Material

Sedimentary Inputs to the Nankai Subduction Zone:

The Importance of Dispersed Ash

Rachel P. Scudder, Richard W. Murray, Steffen Kutterolf, Julie Schindlbeck, Michael B. Underwood, Kuo-Lung Wang

Sources of volcanic ash to the Nankai region

This section of the Supplemental Material is related to Section 2 of the main text.

Shikoku Basin Paleogeography

The Shikoku Basin formed between 30 and 15 Ma due to back-arc rifting and seafloor spreading in the eastern part of the Philippine Sea plate (Taylor, 1992; Sdrolias et al., 2004; Pickering et al., 2013). Since its formation, the history of the Shikoku Basin has been complex (Figure S1). During the Neogene alone it is thought that six main tectonic events occurred (Kano et al., 1991; Taira, 2001). First rifting of the paleo-Izu-Bonin Arc and opening of the Shikoku Basin via seafloor spreading has been interpreted as occurring from ~25 to ~15 Ma. Following or coincident with the rifting of the paleo-Izu-Bonin Arc, rifting of the paleo-Honshu continental arc and spreading of the Japan Sea basin is believed to occur from ~22 to ~15 Ma. The rifting caused Japan to break away from Eurasia, and SW Japan (Honshu) to rotate clockwise ~45° as it drifted south (Kimura et al., 2005; Pickering et al., 2013). From ~17 to ~12 Ma the SW Honshu arc exhibited widespread, near-trench igneous activity. At ~15 Ma the initiation of subduction of the Philippine Sea plate and collision of the Izu-Bonin Arc against the SW Honshu Arc is thought to have occurred, and was followed by a major episode of

¹Supplemental Material. Figures, tables, and calculations. Please visit <https://doi.org/10.1130/GES01558.S1> or the full-text article on www.gsapubs.org to view the Supplemental Material.

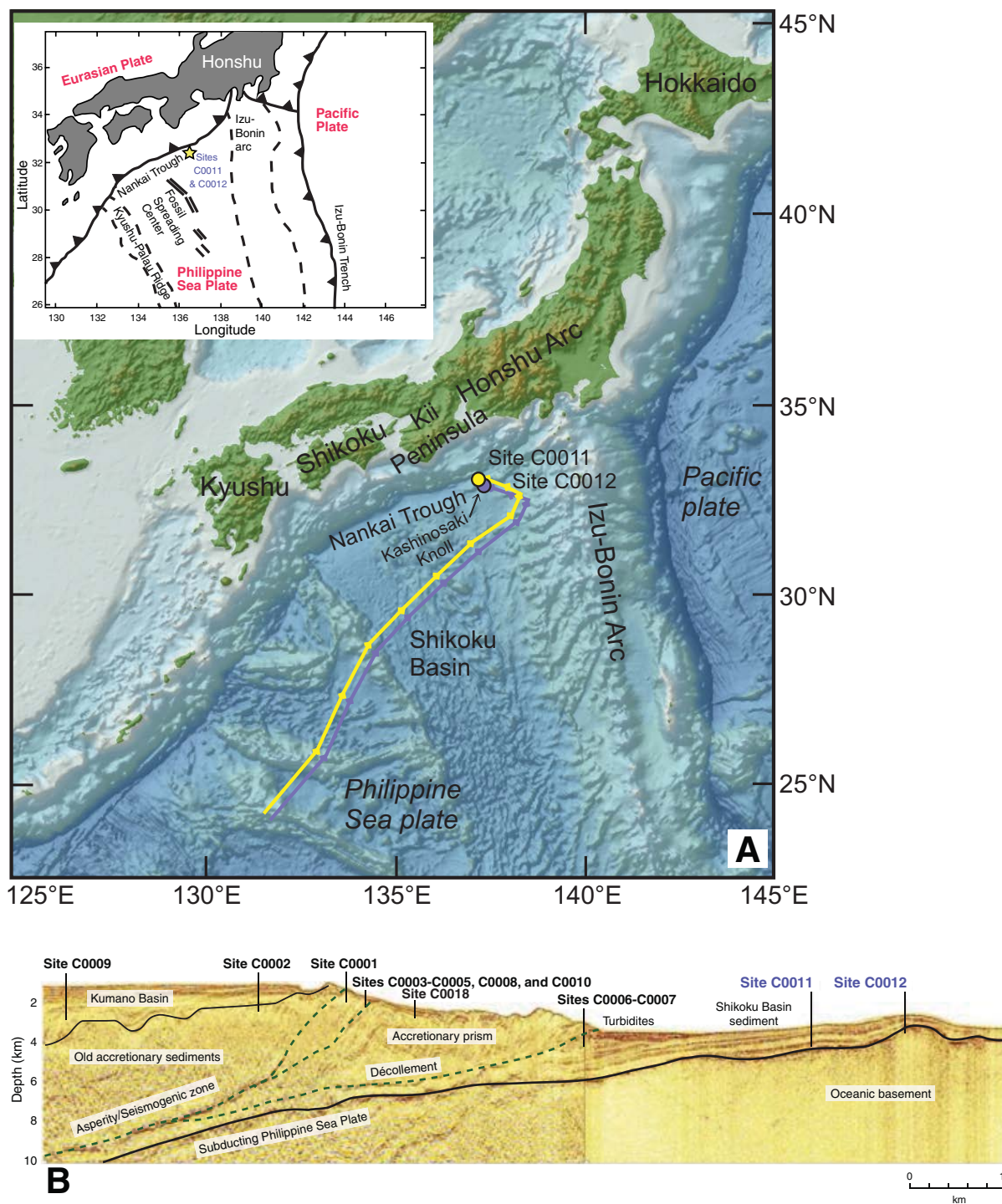


Figure 1. (A) Locations and backtrack paths for Integrated Ocean Drilling Program (IODP) Sites C0011 (32.82906, 136.8820833) and C0012 (32.7481, 136.91736166). Backtrack paths are shown for 20 Ma for each site. Tick marks represent 2 Ma increments. Map created using GeoMapApp (<http://www.geomapapp.org>; GMT-Global Multi-Resolution Topography; Ryan et al., 2009). Paths generated from GPlates are set relative to the fixed reference frame of the Earth's spin axis (Gurnis et al., 2012). Inset after Henry et al. (2012b). (B) Spliced composite profile of a representative depth section from the Nankai Trough Seismogenic Zone Experiment (NanTroSEIZE) 3-D data volume (Moore et al., 2009) and Line 95 from IFREE mini-3-D seismic survey (Park et al., 2008). Projected positions of Stage 1 and 2 drilling sites, including Sites C0011, and C0012, are shown (from Henry et al., 2012a).

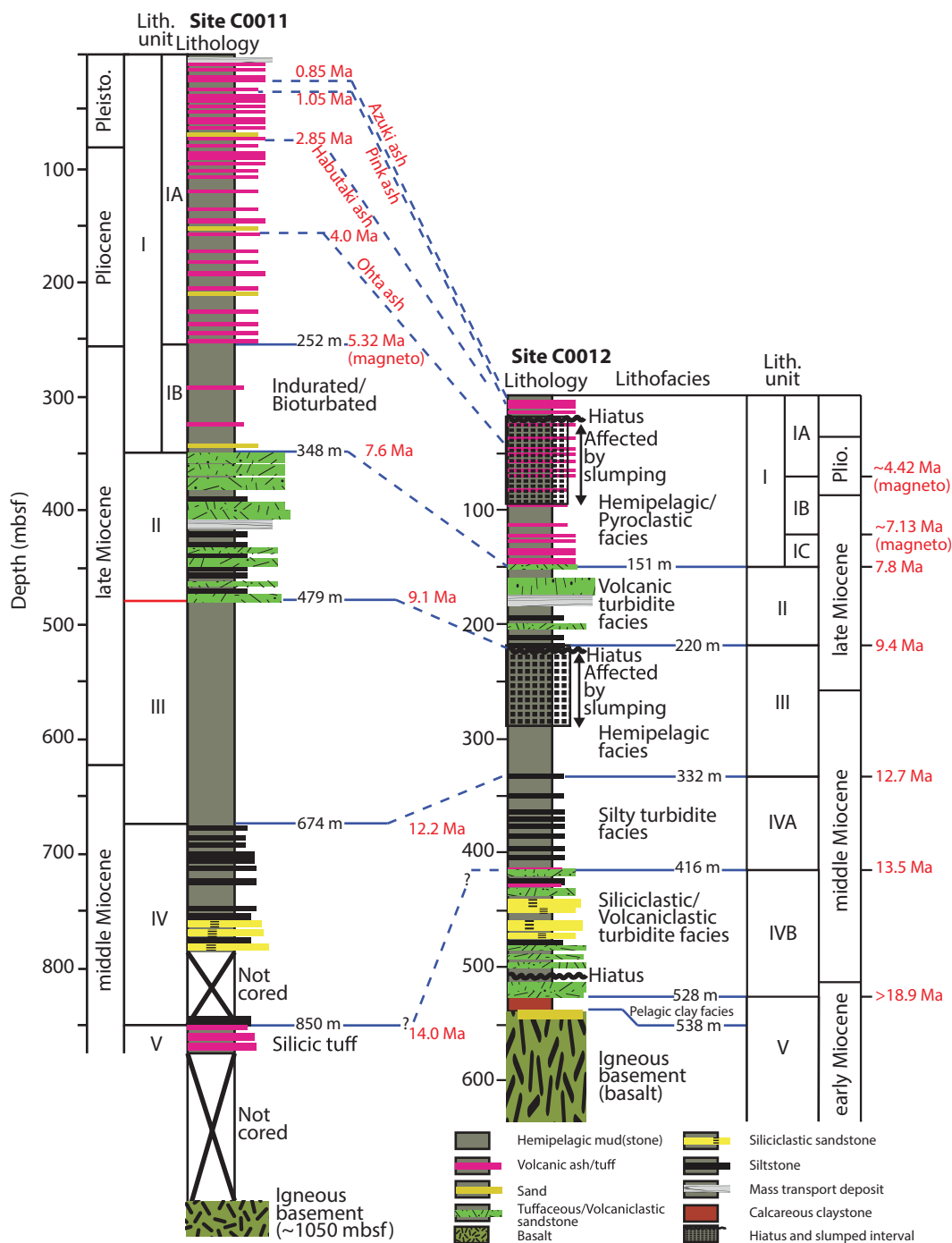


Figure 2. Lithologic columns for Sites C0011 and C0012 based on results from Expeditions 322 and 333. After Henry et al. (2012a). Unit I (0 to ~348 meters below seafloor (mbsf) at C0011; 0 to ~151 mbsf at C0012) corresponds to ash-rich, fine-grained hemipelagic material with the abundance of ash layers and fresh glass shards decreasing downcore. There are many discrete ash layers within this hemipelagic-pyroclastic facies. The boundary between Units I and II is marked by an abrupt appearance of volcaniclastic and tuffaceous sandstone turbidites interbedded with dark gray clayey siltstone. Unit II (volcanic turbidite facies) spans from ~348–479 mbsf at Site C0011 and from ~151–220 mbsf at Site C0012. Unit III (C0011: 479–674 mbsf; C0012: 220–332 mbsf) is characterized by bioturbated hemipelagic claystones. Unit IV (~674–850 mbsf at Site C0011; ~332–416 mbsf at Site C0012) is a silty turbidite facies of bioturbated mudstone with interbeds of normally graded siltstone and fine-grained siliclastic sandstone. Unit V contains tuffaceous sandy mudstone and sandstone, with minor amounts of tuff (Pickering et al., 2013). Unit VI is a thin pelagic claystone facies that rests on basalt basement at ~538 mbsf at Site C0012. At Site C0011, basement was not reached (coring stopped at ~881 mbsf; Saito et al., 2010, and Henry et al., 2012a).

Glass shards from select ash layers (52 layers from Site C0011 and 28 layers from Site C0012) were analyzed for major elements by electron microprobe (EMP) at the Research Center for Marine Geosciences (GEOMAR) (Kiel, Germany) as reported here (Table S2 [footnote 1]) and in Kutterolf et al. (2014). A further subset of glass shards from six ash layers from Site C0011 and five ash layers from Site C0012 (Table S3) were analyzed for trace elements by laser-ablation-ICP-MS (LA-ICP-MS) at National Taiwan University and are from Kutterolf et al. (2014). The methods for EMP and LA-ICP-MS are given in Kutterolf et al. (2011, 2014) and Schindlbeck et al. (2015). Based on their major and trace element chemistry (particularly Ti, Mg, Cr, Sc, and La), two ash layers, C0012C-1H-3 (116–118 cm) and C0011D-4H-2 (53–55 cm), were identified as representative of dacitic and rhyolitic ash layers at these sites for inclusion in the statistical models.

Drift-corrected calibrations were generated using the international Standard Reference Materials (SRMs) AGV-1, BCR-2, BIR-1, DNC-1, MAG-1, PACS, and W-2; prepared and analyzed identically as, and along with, the natural samples. Precision was quantified by repeated preparations and analyses of the international SRM BHVO-2, and is better than 2% of the measured values for all the major elements (except for Na, K, and P), Sc, Sr, Nb, Pr, Eu, Gd, Er, Hf, Ta, Th, and U; between 2%–5% for Na, K, V, Ni, Cu, Rb, Zr, Ba, La, Ce, Nd, Sm, Tb, Dy, Ho, Yb, and Lu; and between 5%–10% for P, Sn, Cs, and Pb. Accuracy was compared to independent analyses of BHVO-2 that were included in each batch as unknowns. Accuracy was within the precision of the analyses.

Dry bulk-density values were calculated from shipboard moisture and density measurements (Saito et al., 2010; Henry et al., 2012a). Depositional ages were calculated by fitting linear segments to the respective age-depth models (Henry et al., 2012a), solving for the slope of each line segment, and then computing the age for each depth point on that segment.

5. GEOCHEMICAL AND STATISTICAL APPROACH

We applied multivariate statistical treatments to our geochemical data set (Table S1 [footnote 1]) in order to identify the number and composition of the sources to the bulk sediment. We used the Q-mode factor analysis (QFA) and constrained least squares (CLS) multiple linear regression techniques from Piasias et al. (2013) and the CLS optimization methods of Dunlea and Murray (2015). These approaches are derived from Leinen and Piasias (1984, and references therein), Kyte et al. (1993), and other researchers, and have been used successfully by our research group in a number of geological and oceanographic settings (e.g., Martinez et al., 2007, 2009, 2010; Ziegler et al., 2007, 2008; Ziegler and Murray, 2007; Scudder et al., 2009, 2014, 2016; Dunlea et al., 2015a, 2015b). QFA helps to identify objectively the number of independent components in the sediment, although the lithologic compositions of these components calculated do not necessarily represent the exact, specific composition of any individual end-member (Piasias et al., 2013). In CLS analysis, the composition of potential end-members are mixed until the best statistical solution is reached. Thus, QFA generates an objective assessment as to the number of

generic geologic sources and their broad composition(s) and CLS tests for the quantitative mix of specific sources.

Based on previous work in northwest Pacific pelagic sequences that contain arc-derived ash (Scudder et al., 2009, 2014, 2016), we used a refractory suite of elements predominantly associated with aluminosilicate components (Al, Ti, Sc, Cr, Nb, La, Th). The number of elements that can be used is scaled according to the number of samples in the data set (e.g., Reimann et al., 2002; Piasias et al., 2013), and this particular element menu is used because we are targeting *only* aluminosilicate end-members in this study (ash, crustal sources, etc.). Being aluminosilicates, the end-members of interest fall in the compositional spectrum between, including upper crustal (e.g., loess, continental crust, and ashes of felsic to dacitic composition, etc.) as well as more primordial sources (basalts, etc.). We are not interested in the oxide component, biogenic material, and so on, and therefore elements such as Fe, Mn, Ca, Si, and P (and others) are not incorporated into the statistical modeling. Such components may be potentially important to studies interested in the complete composition of the sedimentary sequence, but are not relevant to our study here that focuses on the aluminosilicate fraction (terrigenous material and volcanic ash, transported via various pathways as discussed throughout this paper).

Resolving specific geologic sources within the upper crustal group of potential geochemical end-members contributing to the aluminosilicate fraction of the sediment is particularly challenging. In addition to the ash layer compositions sampled from a given site, the compositions of additional generic end-members were identified from the literature (Table S4 [footnote 1]). Identification of eolian and continental crustal-type sources contributing to the aluminosilicate fraction is relatively straight forward, and can be reasonably compiled from “representative” data such as “Chinese Loess” (Jahn et al., 2001), “Upper Continental Crust” (UCC, Taylor and McLennan, 1985), and “Post-Archean average Australian Shale” (PAAS, Taylor and McLennan, 1985). Identification of potential volcanic sources with broadly intermediate compositions (e.g., dacites) and the composition of older material is more difficult due to the number of likely sources and the potential for geochemical evolution of a source through time (as is the case with all provenance studies regardless of approach). Finally, it is impossible using these methods to discriminate between the primary chemical fingerprint of a specific volcanic product (e.g., Kyushu Rhyolite) and chemically equivalent (with respect to the refractory element menu we use) alteration products of the same volcanic source. This will be elaborated upon later in this paper.

6. QUANTIFICATION OF DISPERSED ASH ENTERING THE NANKAI SUBDUCTION ZONE

6.1. Overview

Moving beyond the previous work of Scudder et al. (2016) we considered two closely related strategies in our assessment of the dispersed ash. First, we

considered Sites C0011 and C0012 as one data set, that is, as together representing the average input to the Nankai system. Secondly, we also considered the two sites each as individual data sets. The first approach is considered because, given their proximity to each other, both sites likely share similar histories of eolian input. The two sites most likely also have been similarly influenced by surface currents and other oceanographic features over time (e.g., position relative to the core of the Kuroshio Current, direction of bottom water circulation, etc.).

The second approach provides further resolution of the differences between the two sites, which is appropriate given their different stratigraphies (Fig. 2). Secondly, there is a 550 m bathymetric depth difference, at least at the current time. Thirdly, there is a difference in the numbers of ash layers. If all of the layers are air fall derived, the number of ash layers should be relatively similar (perhaps with some small differences due to reworking). That the occurrence of discrete ash layers is different may also be reflected in the dispersed ash. Finally, there are observed differences in the microprobe analyses of the discrete ash layers (Table S2 [footnote 1]). As will be evident from the discussion below, both approaches yield similar outcomes, and together present a comprehensive quantification of the composition of the different sources entering the Nankai subduction zone.

6.2. Considering Both Sites as a Single Representative Average Subduction Input

6.2.1. Identification of the Number of Sources

The QFA results from the two sites together (117 samples total) indicate that there are four sources that explain 99% of the total variability in the data set, with the individual sources explaining 29%, 13%, 41%, and 16% of the variability respectively. This does not mean that there could not be five or more sources, but additional sources are not *required* to completely explain variability within the data set. For example, when QFA is forced to a five-component model, the fifth end-member explains <1% of the variability while the overall model does not improve significantly (that is, it continues to explain 99% of the variability). Furthermore, it does not mean that all four sources are present in each sample, as the statistical analysis is considering the entire data set without consideration of source evolution or the complete turning on/off of any geological inputs.

6.2.2. Identification of the Composition and Abundance of the Sources

The CLS multiple linear regression confirms that there are four sources to the sediment in the combined model and provides the best estimation of their composition and specific origin (Fig. 3). We statistically tested combinations of likely inputs derived from the literature, taking into account the approxi-

mate compositions provided by QFA (Table S5 [footnote 1]), and by making assumptions based on geological constraints as to where the sources are most likely to have been located (Table S4). Our statistical treatments consider in sequence all potential combinations of end-members contained in the aluminosilicate fraction and rank them according to their statistical strength (Dunlea and Murray, 2015). Of the top ten models produced by the CLS output we have taken the average of eight of them (Table S6). Two models were excluded because: (1) they did not contain a dust source, which given the location of the sites we assume must be present, (2) they contained a significant portion of mafic ash (material from the Izu-Bonin Front Arc [IBFA]), which is inconsistent with the sedimentological observations from these sites, and (3) the output of these two models was very noisy in comparison to the other eight models and with the sedimentological observations.

We consider first the inferred “Asian dust” source. Here, it is important to recall that we are using known end-member compositions as approximations of potential inputs. Of the eight models used in the overall average, six of them indicate that the eolian input is best represented by the composition of “Chinese Loess” of Jahn et al. (2001), whereas two suggest that PAAS of Taylor and McLennan (1985) provides a better fit. Given the interdependencies of the CLS modeling, namely that the end-member compositions of the other non-crustal end-members will statistically influence the composition of this first end-member, this consistent outcome clearly indicates that the Asian Dust component is best represented by a general crustal composition akin to “Chinese Loess” and “PAAS.” This, of course, is by no means a new finding, but that the model outputs are so consistent in this regard gives increased confidence in our approach. These results indicate that Asian Dust represents the highest abundance of sources to the sediment with abundances ranging from 48 to 77 wt% of the total sediment at both sites (Table S7 [footnote 1]).

This Asian Dust source is more likely to have been transported by wind rather than by erosion from the nearby terrestrial sources, although we cannot discount a partial erosional pathway, even for some of this source’s journey. For example, soils from Japan are predominantly composed of eolian dust transported from the Chinese Loess Plateau, the Gobi Desert, Mongolia, and surrounding regions (e.g., Inoue and Naruse, 1987; Feng et al., 2011), and erosional products from such soil could be transported to Sites C0011 and C0012.

We now turn to the three other end-members, which we interpret as quantifying three different ash contributions. For example, the second end-member in six of the models includes what we have labeled as “Rhyolitic Ash,” which is the composition of the most felsic ash layer found at Sites C0011 or C0012, as mentioned earlier. Andesite from the Izu-Bonin Arc appears in the remaining two models for this second end-member. Therefore, we interpret that the composition of this dispersed ash component is a “rhyolitic-andesitic” ash, and is probably toward the rhyolitic end of this spectrum. Because this dispersed source overall matches well with the “Rhyolite” ash layers, we interpret that a portion, or even all, of this dispersed ash component is the result of ash that was transported through the atmosphere as an admixture of ash from the Izu-Bonin island arc.

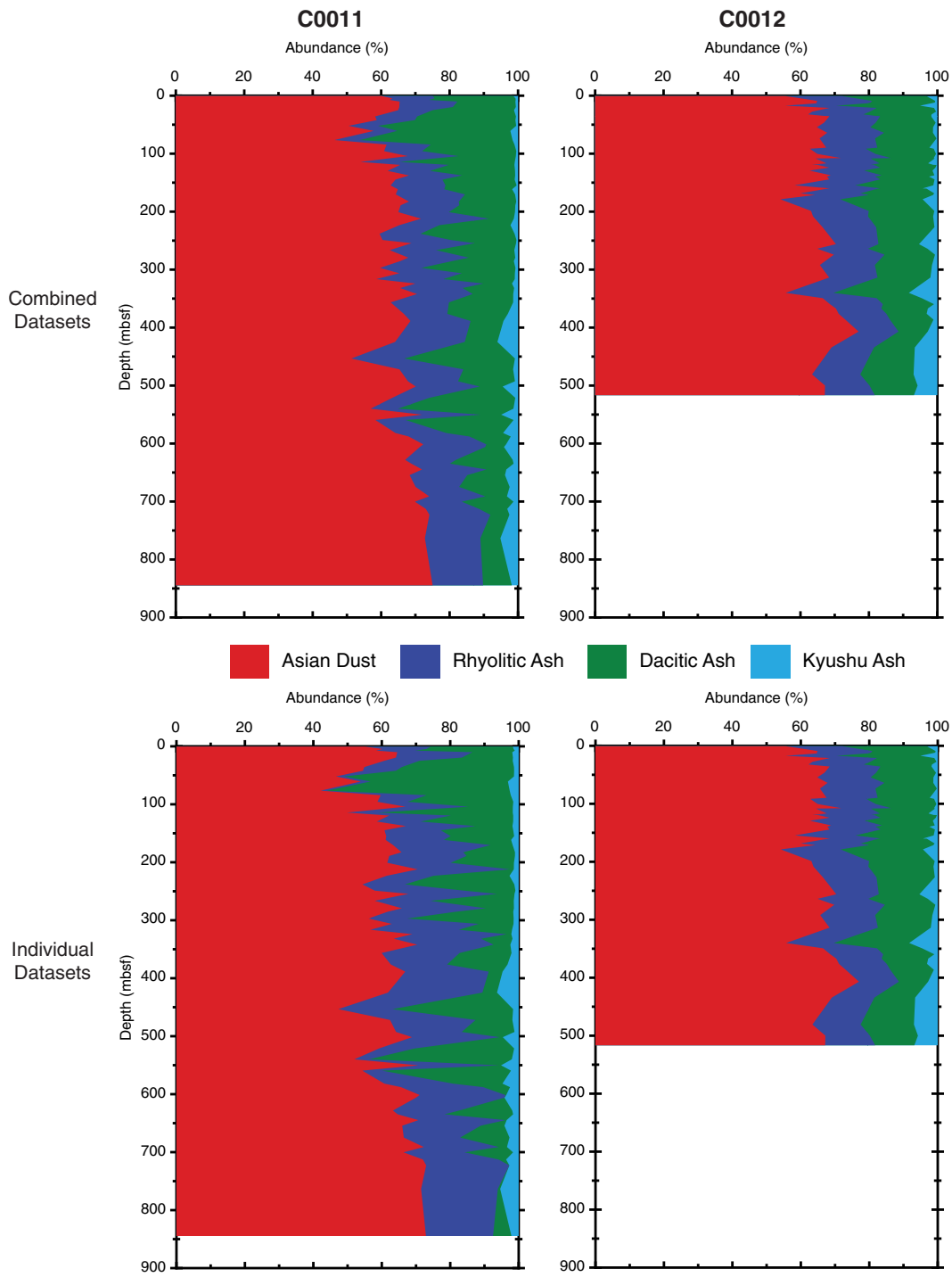


Figure 3. Abundance (wt%) of sources identified by constrained least squares multiple linear regressions. mbsf—meters below seafloor.

For the third end-member, four models yield Izu-Bonin Dacite, two models include dacite from the Honshu Arc, and two models suggest “Honshu Rhyolite.” We call this end-member “Dacitic Ash” to differentiate it from the “Rhyolite” of the second end-member. While the compositional differences between the second and third end-members may appear slight, they are statistically required and do indeed show a composition contrast, with the second end-member being predominantly rhyolitic, and the third predominantly dacitic.

For the fourth end-member, all eight models include material from the Kyushu Arc, with four of them yielding “Kyushu Dacite” and four models indicating “Kyushu Andesite.” We interpret that this fourth end-member clearly is uniquely from Kyushu and is intermediate in composition.

Considering the abundances of the three ash sources for Site C0011, the “Rhyolitic Ash” ranges from 8 to 20 wt%, the “Dacitic Ash” ranges from 5 to 34 wt% and is of lesser importance deeper in the site, and the “Kyushu Ash” ranges from 0 to 6 wt% and is of greater importance deeper in the site. Broadly, Site C0012 presents the same overall patterns as does Site C0011, although stratigraphically compressed. The modeling indicates, therefore, that the total dispersed ash components comprise 23–49 wt% of the bulk sediment at the two sites.

6.2.3. Potential Transport Pathway

As discussed previously, both sites are currently located relatively near to mainland Japan and the Nankai accretionary prism and, thus, when considering the four end-members we must take into account potential influxes eroded from these and other terrestrial sources (e.g., Pickering et al., 2013). In this discussion, we emphasize that geochemical composition alone does not yield information regarding the pathway or physical agent by which particles are transported to a given location, and that the main focus of our study (quantifying the abundance and composition of the dispersed component) is independent of the specific pathway of ash incorporation into the sediment and/or alteration.

In this context, because the “Dacitic Ash” and “intermediate Kyushu Ash” components do not appear in the measured discrete layers, we interpret that their most recent source is more likely to be erosional, although a portion of them could be transported through the atmosphere as well. An alternative, yet untestable, interpretation would be that these sources were originally airfall ash that resulted in very thin layers that have subsequently been mixed (e.g., bioturbated) into the bulk sediment. However, we favor a non-airfall pathway because ash transport by density currents has been shown to be important at these locations (e.g., Schindlbeck et al., 2013; Kutterolf et al., 2014), with the respective dilute suspension clouds perhaps also providing variable input for the dispersed ash component. Therefore, we collectively interpret that the results from the modeling based on both Sites C0011 and C0012—being considered together—are most consistent with the “Rhyolitic Ash” being from subaerial transport, the “Dacitic Ash,” and “Kyushu Ash” being eroded from

terrestrial or uplifted accretionary-prism sources, and the “Asian Dust” composition being transported by wind with perhaps some eroded from terrestrial or prism sources.

6.3. Considering Sites C0011 and C0012 as Separate Data Sets

Overall, the combined models considering Site C0011 and C0012 together provide a strong record of the overall input into the Nankai subduction zone. Given the possible differences in the sites, as discussed above, performing statistical analysis on the Sites C0011 and C0012—separately from each other—can allow us to further characterize the detailed sources to the sediment in this region.

6.3.1. Site C0011

QFA of the data from Site C0011 indicates that four factors are the minimum required to explain 99% of the variability of the bulk sediment (Table S5 [footnote 1]). Following an approach analogous to the above discussion of the combined data set, the CLS multiple linear regression identifies that the aluminosilicate component of the bulk sediment is best described with the four sources being compositionally modeled by a mixture of “Asian Dust,” a “Rhyolitic Ash,” “Dacitic Ash,” and “intermediate Kyushu Ash” (Fig. 3; Table S8A).

The “Asian Dust” component represents the highest abundance of sources to the sediment with abundances ranging from 42 to 73 wt%, which is consistent with the combined model. The “Rhyolitic Ash” is entirely modeled by inclusion of the “Rhyolite” ash layer, and ranges from 2 to 28 wt% at Site C0011. The “Dacitic Ash” is widely variable ranging from 0 to 53 wt%. The “Kyushu Ash” component at Site C0011 ranges from 1 to 6 wt%. Together these three types of dispersed ash and/or clay minerals with comparable geochemical signatures comprise 38 ± 7 wt% of the bulk sediment. This value is consistent with the 23–49 wt% found with the combined model.

6.3.2. Site C0012

Applying the same approaches to Site C0012, QFA indicates that four factors explain 99% of the variability in the bulk sediment. The compositions yielded by these factors suggest that two intermediate and two felsic end-members comprise the aluminosilicate component (Table S5). As with the combined model and specific Site C0011 model, the CLS regressions for Site C0012 indicate that these end-members are best explained by mixing “Asian Dust,” “Rhyolitic Ash,” “Dacitic Ash,” and “Kyushu Ash.” These three dispersed ashes contribute a total of 34 ± 4 wt% of the bulk sediment (Table S8B). Further details of these models can be found in the Supplemental Material (footnote 1).

The “Asian Dust” ranges from 54 to 77 wt% of the aluminosilicate portion of the bulk sediment. The Rhyolitic Ash component is relatively constant, ranging from 12 to 18 wt% of the sediment. As with Site C0011, we interpret that at a portion, or all, of this volcanic “Rhyolite” is the result of transport through the atmosphere. The “Dacitic Ash” component at Site C0012 comprises 9–25 wt% of the bulk sediment. The “Kyushu Arc” dispersed component ranges from 0 to 8 wt% of the sediment at Site C0012 (Fig. 3).

Overall, as with the combined model discussed in Section 6.2, the model that best explains the composition of the sediment at both Sites C0011 and C0012 includes an end-member based on the chemistry of the discrete ash layers (Tables S2 and S3 [footnote 1]). We therefore interpret that a portion, or even all, of the “Rhyolitic Ash” dispersed ash component at each site is the result of ash that was transported through the atmosphere. Analogously, because none of the end-members that make up the “Dacitic” or “Kyushu Ash” components appear in discrete layers, we interpret that they are more likely to be erosional or transported by density currents (e.g., Schindlbeck et al., 2013; Kutterolf et al., 2014), although a portion could be transported through the atmosphere as well. This is consistent with other studies of the tuffaceous and volcanoclastic sandstones, which outline mixed origins for the volcanic material from both the Izu-Bonin and Honshu arcs (e.g., Kutterolf et al., 2014; Pickering et al., 2013; Schindlbeck et al., 2013).

7. DIFFERENTIATION OF ALTERED AND UNALTERED ASH

7.1. Evidence from Smear Slides and Sedimentary Geochemistry

Our combined geochemical and statistical technique is based on a suite of elements that are relatively immobile during diagenesis and alteration beneath the seafloor, and therefore can target variations in provenance. A limitation of this approach, as illustrated above, is that alone it cannot differentiate between altered and unaltered ash.

To address this ambiguity we qualitatively compare the smear slide data with the geochemical-statistical results. If we consider the modeled dispersed ash to be the “sum of altered and unaltered ash, including clay-mineral weathering products of ash,” and the ash described in smear slides as “volcanic glass and volcanic lithics” to be only the “unaltered fraction,” then by difference we can perhaps document at least changes in the trends of the altered dispersed ash. This comparison itself is challenging because fresh volcanic matter smaller than ~10 μm cannot visually be distinguished from clay or other material (fresh or altered), whereas the geochemical-statistical technique includes all grain sizes. Nonetheless, the comparison is informative.

Using this approach, at Site C0011 we observe that the smear slide sum of glass and volcanic lithics is variable, but high (~40% on average), in Unit I (0–348 mbsf) and the upper portion of Unit II (348 to ~400 mbsf), and that below ~400 mbsf the smear slide–based abundances decrease to an average of ~10% and remain low throughout Unit III (479–674 mbsf) and Unit IV (674–850 mbsf).

The total abundance of dispersed ash from our geochemical-statistical approach is ~38% of the bulk sediment and is fairly regular through all units with the exception of a slight peak (~50%) from ~400–500 mbsf. We interpret these trends and virtually identical absolute abundances to indicate that in Unit I at Site C0011 the dispersed ash component is dominated by unaltered ash.

At Site C0012 the volcanic glass and volcanic lithics are lower in abundance throughout the entire sequence. In Unit I and the upper portion of Unit II (to ~150 mbsf) the glass and lithic abundance is ~25% and exhibits high variability. The abundance (~15%) and variability of the glass and volcanic lithic component is low through Unit II and the upper portion of Unit IV (from ~150–400 mbsf), and then increases again to ~25% with more variability in the lower portion of Unit IV. The total dispersed ash abundance at this site is ~34%, with a decrease from ~350–425 mbsf. These results suggest that Unit I of Site C0012 is comprised of a mix of altered and unaltered ash with slightly more altered material in some portions. The altered material is responsible for the ~9–10 wt% difference between the smear slide data and the dispersed ash model results, and indicates that some of the ash component identified in the model is “altered dispersed ash” (that still retains its refractory chemical signature). Some of these slight contrasts with Site C0011 may reflect that Site C0012 is located atop a bathymetric knoll, which may affect the transport or reworking of coarser grained material. In Unit II at both sites the abundance of the altered component increases such that the lower portion of each site appears to include significant amounts of altered dispersed ash.

7.2. Insights from Pore-Water Chemistry

Shipboard interstitial water analyses from Expeditions 322 and 333 pointed toward the alteration of ash as a mechanism for various changes in the dissolved interstitial water chemistry (Saito et al., 2010; Henry et al., 2012a). In particular, dissolved Mg and K are commonly consumed by clays during alteration of igneous basement or ash throughout the sediment column (e.g., Gieskes et al., 1990). In sediments with little to no ash, basement alteration characteristically leads to decreases in Mg and paired molar increases in Ca, reflecting the release of Ca and uptake of Mg during basalt alteration. This is reflected in the Ca profiles at Sites C0011 and C0012 (Fig. 4), and because the basaltic crust is relatively young (~20 Ma; Okino et al., 1994) the basalt is likely still undergoing active alteration. Additionally, $^{87}\text{Sr}/^{86}\text{Sr}$ ratios in the pore water is controlled by mixing of modern seawater, strontium from alteration of volcanic ash, and basaltic basement (Joseph et al., 2013; Torres et al., 2015; Sample et al., 2017).

The Mg and K profiles at these sites, however, while indeed recording continual decreases with depth, reach their lowest (and near-zero) values well within the sediment column (Fig. 4). The depths of Mg and K reaching lowest values, and staying low for the remaining depths of the sequence, are much shallower than the Ca pore-water maxima nearest the basement. However, were Mg and K uptake controlled solely by basement alteration, their profiles (particularly of Mg) should be the molar inverse of the Ca release and thus

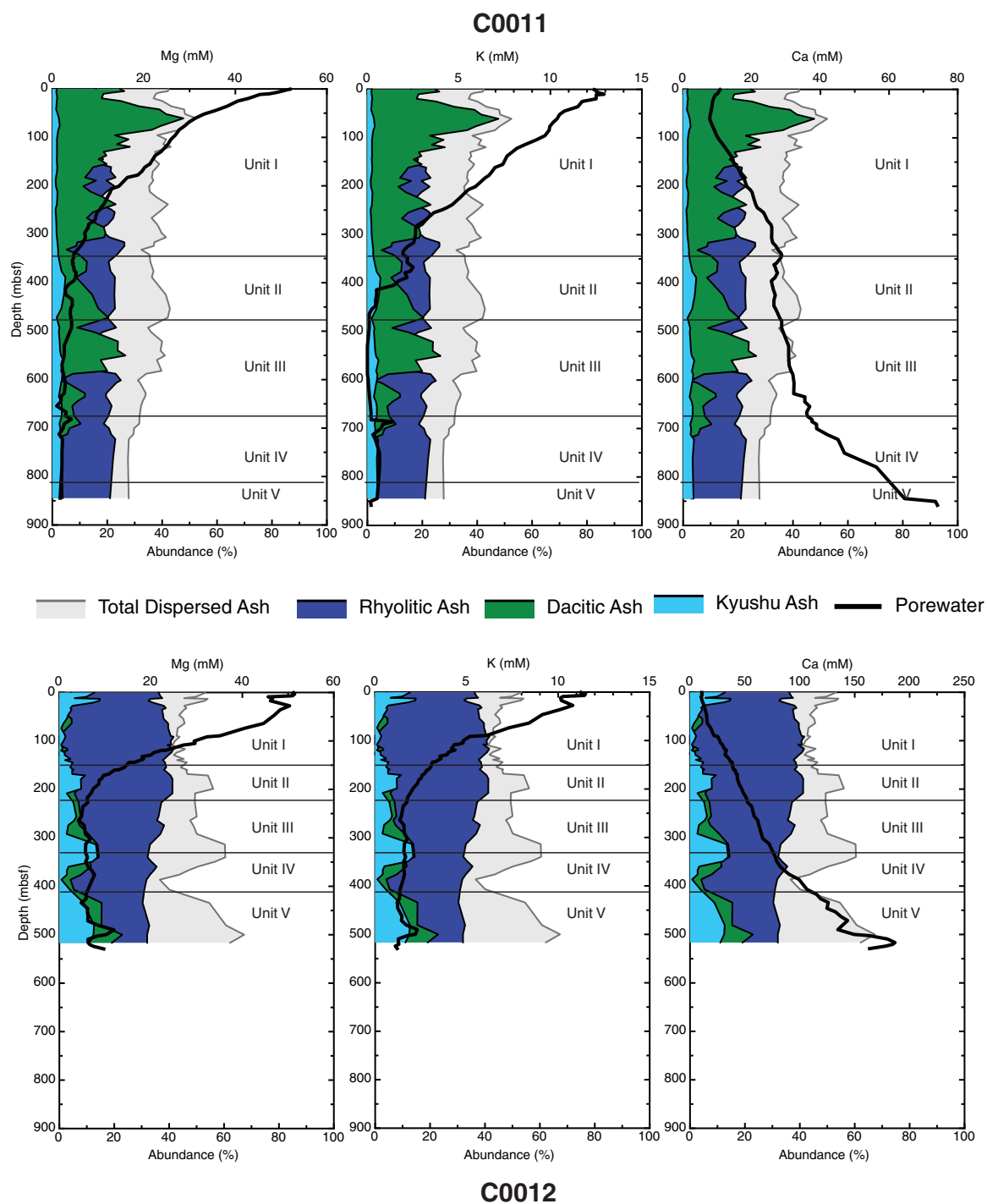


Figure 4. Comparison of dispersed ash abundance (wt%) with pore-water profiles (gray lines) of dissolved Mg (left), K (center), and Ca (right), all in units of mM. Note differences in mM scale between the Ca plots. Pore-water data from Saito et al. (2010) and Henry et al. (2012a). Abbreviation: mbsf—meters below seafloor.

should continue to decrease to the basaltic basement itself (at ~1050 mbsf at Site C0011 and ~538 mbsf at Site C0012). This, along with the curving of the profile, indicates that the volcanic ash found *within* the sediment (both the layers as well as the dispersed ash) is significantly influencing the distributions of dissolved K (and Mg). That is, the ash alteration in the sediment column is consuming the dissolved Mg and K in addition to the deeper basement alteration.

7.3. Summary: Ash Layers and Trends in Alteration

The decrease in ash layers through Unit II (Figs. 4–6) is consistent with “diagenetic alteration loss” of the visually apparent glass shards and min-

ute volcanic fragments (Fig. 5). This interpretation is supported by the ash alteration front found at the top of Subunit IB (~252 mbsf) at Site C0011 and near the Subunit IB/IC boundary (~123 mbsf) at Site C0012. Additionally, there is a sharp variation of porosity and electrical resistivity through the same interval (Saito et al., 2010). Dissolved silica concentrations also decrease, indicating on-going alteration (Henry et al., 2012a).

These findings are also consistent with previous work elsewhere in the Nankai region, which identified removal of K and Cl by alteration of volcanic ash well above the basement at Ocean Drilling Program (ODP) Site 808 (Masuda et al., 1993; Underwood and Pickering, 1996). Additionally, at ODP Sites 808, 1173, and 1177, as well as at Sites C0011 and C0012, anomalous porosity and other properties are caused by small amounts of amorphous silica cement

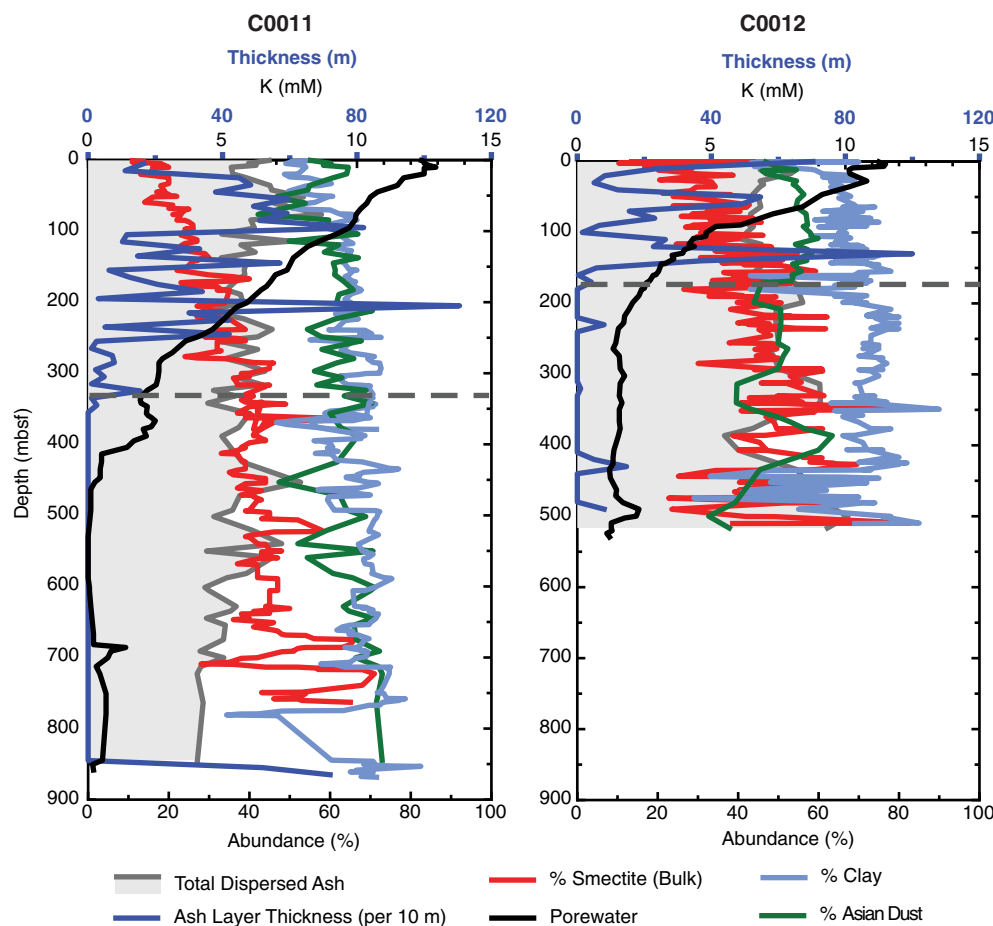


Figure 5. Diagram of the inter-relationships between the K pore-water profile (black line, mM) and ash layer thickness per 10 m (navy blue line, m), plotted against parameters associated with the abundance of material in the bulk sediment at Sites C0011 and C0012. Total abundance dispersed ash (gray shaded line, %), post-Archean average Australian shale (PAAS) from constrained least squares (CLS) (green line, %), smectite component (red line, %), and total clay minerals (light blue line, %). Dashed gray line represents approximate location of alteration front. Smectite and total clay data compiled from Underwood and Guo (2013, 2017).

attributed to “disseminated volcanic glass shards” rather than biogenic opal (Spinelli et al., 2007; White et al., 2011; Hüpers et al., 2015).

■ 8. QUANTITATIVE IMPORTANCE OF DISPERSED VOLCANIC ASH

8.1. Temporal Patterns in Ash Layer Accumulation and Dispersed Ash

We compare the mass accumulation rate (MAR, g/cm²/ky) of the dispersed ash component to a number of common ash layer parameters, including the number of ash layers per unit time, the thickest ash layer per unit time, and the total thickness of ash layers per unit time (Fig. 6). We binned the ash layer data into 0.2 Ma long quanta of “unit time,” to generate a discrete ash layer data set of approximately the same temporal resolution as that of the dispersed ash record. Given the need to temporally “bin” the data set, along with the large effect that short-duration variability would have on a statistical comparison of a small, binned data set, we limit our interpretations to be accordingly qualitative.

At Site C0011 the dispersed ash MAR in Unit I appears to best correlate with “thickest layer” in Unit I (Fig. 6). This relationship suggests that it is eruption volume, rather than frequency, that drives the dispersed ash accumulation. Thick ash layers may result from a large eruption, a relatively nearby eruption, or a combination of the two. In contrast, in Unit I of Site C0012 the dispersed MAR is best correlated to the number of layers and not to either of the “thickness” indicators (Fig. 6). Thus, the dispersed ash component in this unit at Site C0012 may be controlled by the frequency of explosive eruptions to a greater degree than the size of the eruption.

Because both sites are broadly approaching the arc systems through time, one could predict that thicker ash layers would be more prevalent in the younger (shallower) sections of both sites. This is indeed observed in the upper portion of Unit I at Site C0011, but not at Site C0012. This contrast may reflect differences in their depositional location (i.e., Site C0012 atop the bathymetric knoll). Due to the bathymetric influence of the Kashinosaki Knoll, stronger currents could enhance the redistribution of thinner and finer-grained discrete ash layers that arrived initially as suspension fall out. Furthermore, slumping is more prevalent at Site C0012. Regardless, given that the relationship between the thickness-related parameters and the dispersed ash component is not strongly observed in the younger discrete layer record, we suggest the dispersed ash through Unit I is responding to overall volcanic activity rather than specific eruptive events.

Below the Unit I/II boundary—at both sites—the number of ash layers, as well as their thickness, decreases to virtually zero while the dispersed ash remains high (Fig. 6). This may reflect that deeper in these records there are periods where volcanism was reduced as a result of a cessation of subduction or change in angle of convergence of the Philippine Sea plate (Mahony et al., 2011; Kimura et al., 2015). In addition, the sites were influenced by turbidity currents (Units II, IV, and V), or were further away from eruptive fronts (Unit

III), that may have resulted in either fewer and/or thinner layers that would be more susceptible to being mixed away (by bioturbation or otherwise). That the geochemical signal attributed to dispersed ash is high at times with so few ash layers clearly demonstrates that volcanism was present to some degree, although the ash layers may have been very thin and thus altered or erased by bioturbation. The presence of dispersed ash in a sequence without discrete ash layers is also consistent with there being no larger, layer-generating, volcanic eruptions through this time period. Indeed, semi-continuous small eruptions could have supplied the dispersed ash component to the bulk sediment (e.g., Peters et al., 2000), as could other processes such as erosion from terrestrially exposed ash deposits and widespread chemical weathering of volcanic rocks (as noted by the increase in ash bearing turbidites through this time [Pickering et al., 2013]), or subaqueous eruptions (Fig. 7). This interpretation is consistent with the end of the upper Shikoku Basin facies being assigned to the bottom of the last distinct ash layer located in Unit III at Site C0011 (Saito et al., 2010).

8.2. The Total Amount of Dispersed Ash: Mass Balance Comparisons

For each site we calculated the cumulative mass (g) of ash found in the discrete ash layers in a 1 cm x 1 cm vertical column of sediment, and compared that to the cumulative mass of dispersed ash (and altered clay products) in the same 1 cm vertical sediment column. Details of these calculations are in the Supplemental Material (footnote 1). We performed the calculations for two scenarios. First, and most appropriate for our study, we excluded the intervals of tuffaceous sandstone and/or volcanoclastic turbidite material and secondly, for comparison purposes only we include those intervals.

At Site C0011, there is a total of 10.6 m of ash layers, and therefore the above calculations yield ~2500 g/cm² (that is, in the 1 cm sediment column) of ash contained in *layers* from 0 to 878 mbsf. Including the sandstones and turbidites increases this amount to ~12700 g/cm². The *dispersed* ash and alteration products supply an additional 38000 ± 7000 g/cm². At Site C0012, there is a total of 5 m of ash layers, and therefore from 0 to 528 mbsf there is ~1200 g/cm² of ash *layers* (increasing to ~3300 g/cm² with sandstones/turbidites). The *dispersed* ash and alteration products provide 20000 ± 3000 g/cm². Therefore, dispersed ash is contributing a maximum of 15–17 times more than the ash layers (and 3–6 times more if including the sandstones/turbidites), quantitatively indicating that the dispersed ash and related erosional products are far more abundant than the discrete ash layer material.

■ 9. SUMMARY

There is a high abundance of volcanic ash entering the Nankai Trough on the subducting Philippine Sea plate. Smear slide analyses estimate that dispersed ash constitutes between an average of ~7–30 wt%, with wide variabilities and uncertainties throughout the lithostratigraphic units. These estimates

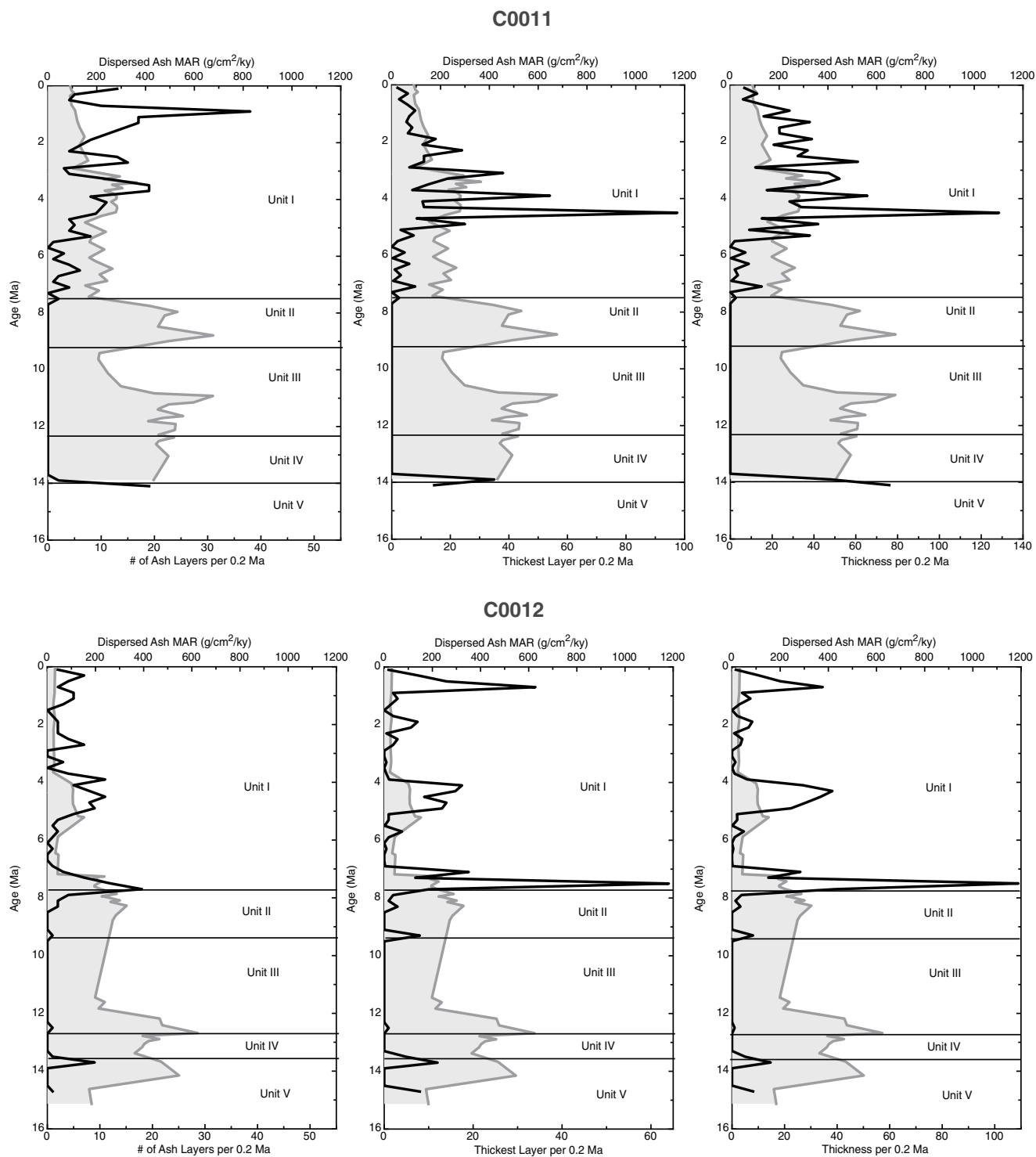


Figure 6. The mass accumulation rate of total dispersed ash (grey shaded line, $\text{g}/\text{cm}^2/\text{ky}$, the same in each panel by site) plotted against parameters associated with the sedimentation of discrete ash layers per 0.2 Ma (black line, parameters are different in each panel as shown in the bottom x-axis labels). A moving 0.2 Ma window was chosen to bin each discrete ash layer parameter to approximate the resolution of the modeled dispersed ash record. Note that while the total thickness of ash layers at Site C0011 (10.6 m) may seem low given the visually high presence of ash layers (337 layers through the depth range of comparison) the average thickness of the ash layers is ~ 3.1 cm, which is consistent with the core descriptions and our own measurements of each ash layer. At Site C0012, these calculations yield an average ash layer thickness of ~ 2.8 cm, which is again consistent. At Site C0011, the curved decrease in Mg flattens to low values at ~ 350 mbsf (for K, at ~ 450 mbsf), while at Site C0012 the decrease in Mg flattens to low values at ~ 200 mbsf (for K, at ~ 250 mbsf). The shallower depths may reflect the higher heat flow at Site C0012.

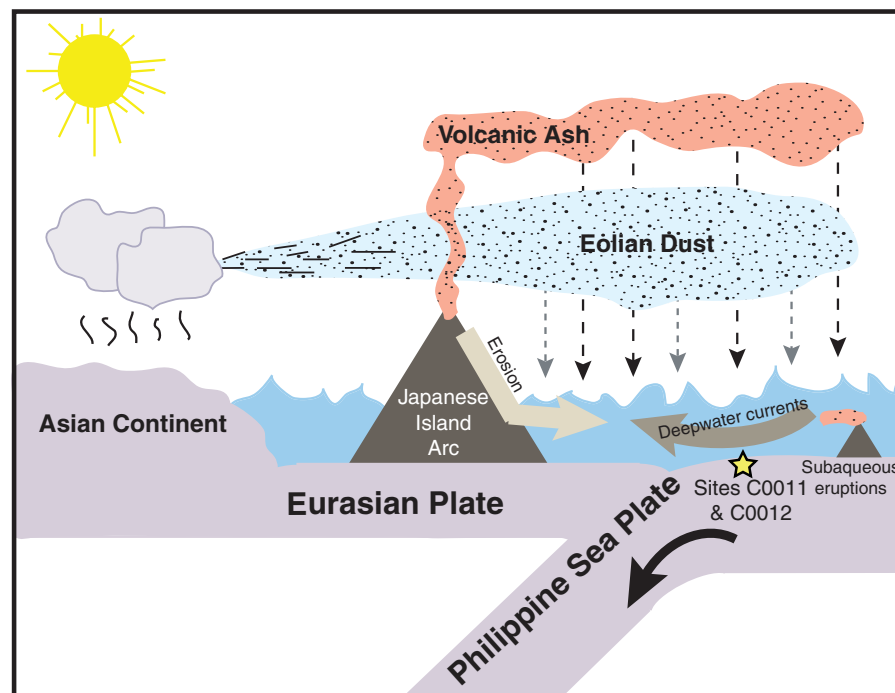


Figure 7. Summary diagram of potential transport mechanisms of the sources to the bulk sediment at Sites C0011 and C0012, Nankai Trough, south of Japan's island of Honshu. Our geochemical and statistical approach indicates that four distinct sources contribute aluminosilicate material to the Nankai subduction zone. One source is Asian Dust, which is more likely to have been transported by wind rather than by erosion from the nearby terrestrial sources. We cannot, however, discount a partial erosional pathway, even for some of this source's journey. There are also three distinct dispersed ash components. These are "Rhyolitic Ash," "Dacitic Ash," and "intermediate Kyushu Ash." The "Rhyolitic Ash" dispersed ash component is the result of ash that was transported through the atmosphere. The "Dacitic Ash" and "intermediate Kyushu Ash" components do not appear in the measured discrete layers, therefore we interpret that their most recent source is more likely to be erosional, although a portion of them could be transported through the atmosphere as well. For all the ash sources, it is possible that some of this material has originated from subaqueous eruption.

of ash importance (as well as those based on ash layers alone), while large, significantly *underestimate* the total amount of total volcanic material entering the Nankai subduction system.

Our geochemical and statistical approach when applied to a combined data set from Sites C0011 and C0012 indicates that four distinct sources contribute aluminosilicate material to the Nankai subduction zone. One source is eolian transported Asian Dust, comprising 48–77 wt% of the bulk sediment. There are also three distinct dispersed ash components. These are "Rhyolitic Ash" (15 wt% of the bulk), "Dacitic Ash" (18 wt%), and "intermediate Kyushu Ash" (2 wt%). Therefore, in total, the dispersed ash components from the combined model represent ~35 wt% of the bulk sediment. The "Rhyolitic Ash" component likely is from eolian transport, while the "Dacitic" and "Kyushu Ashes" are more likely to include an erosional component (Fig. 7).

Individual models of Sites C0011 and C0012 indicate that dispersed ash at Site C0011 accounts for 38 ± 7 wt% of the bulk sediment, and at Site C0012 is 34 ± 4 wt%. Overall, Site C0011 exhibits slightly less variability than Site C0012, although the time-depth patterns in dispersed ash or geochemically similar altered clay material are broadly similar. At Site C0011, the dispersed ash component supplies 38000 ± 7000 g/cm² of material to the Nankai subduction system, whereas Site C0012 supplies 20000 ± 3000 g/cm². These values are enormous

compared to the ~2500 g/cm² (C0011) and ~1200 g/cm² (C0012) of ash in the discrete ash layers (or ~12700 g/cm² and ~3300 g/cm², respectively, if volcanic sandstones and turbidites are considered). Therefore, the total amount of dispersed ash is 15–17 (or 3–6 if volcanic sandstones and turbidites are included) times greater than the amount of ash found in the discrete layers.

Below the Unit I/II boundary at both sites the number and thickness of ash layers vastly decreases while the dispersed ash component remains high (Fig. 5). The mass accumulation rate of dispersed ash at Site C0011 correlates best with "thickest layer" in Unit I, suggesting that eruption volume—rather than eruption frequency—may drive the dispersed ash accumulation through this interval. In contrast, in Unit I of Site C0012, the dispersed ash MAR is best correlated to the number of ash layers rather than "thickness." Pore-water records show that ash alteration is ongoing and is consistent with the decrease in the number and thickness of ash layers at both sites being exacerbated by diagenesis. Together, a holistic assessment of discrete layers, dispersed ash, and alteration products, provides a more complete record of regional-scale volcanic history than any one alone.

As highlighted in Scudder et al. (2016), the use of discrete volcanic ash layers as a stratigraphic and temporal tool has a long and wide-ranging history (e.g., Cambrey et al., 1995; Straub and Schmincke, 1998; Kutterolf et al., 2014),

- Stern, T.A., Stratford, W.R., and Salmon, M.L., 2006, Subduction evolution and mantle dynamics at a continental margin: Central North Island, New Zealand: *Reviews of Geophysics*, v. 44, p. 359, <https://doi.org/10.1029/2005RG000171>.
- Straub, S.M., 2003, The evolution of the Izu Bonin–Mariana volcanic arcs (NW Pacific) in terms of major element chemistry: *Geochemistry Geophysics Geosystems*, v. 4, p. 277, <https://doi.org/10.1029/2002GC000357>.
- Straub, S.M., and Schmincke, H.U., 1998, Evaluating the tephra input into Pacific Ocean sediments: Distribution in space and time: *Geologische Rundschau*, v. 87, p. 461–476, <https://doi.org/10.1007/s005310050222>.
- Taylor, S.R., and McLennan, S.M., 1985, *The Continental Crust: Its Composition and Evolution*: Oxford, UK, Blackwell Scientific Publications, 328 p.
- Tobin, H.J., and Kinoshita, M., 2006, NanTroSEIZE: The IODP Nankai Trough Seismogenic Zone Experiment: *Scientific Drilling*, v. 2, p. 23–27, <https://doi.org/10.5194/sd-2-23-2006>.
- Torres, M.E., Cox, T., Hong, W.-L., Mcmanus, J., Sample, J.C., Destrienneville, C., Gan, H.M., Gan, H.Y., and Moreau, J.W., 2015, Crustal fluid and ash alteration impacts on the biosphere of Shikoku Basin sediments, Nankai Trough, Japan: *Geobiology*, v. 13, p. 562–580, <https://doi.org/10.1111/gbi.12146>.
- Underwood, M.B., and Guo, J., 2013, Data report: Clay mineral assemblages in the Shikoku Basin, NanTroSEIZE subduction inputs, IODP Sites C0011 and C0012, *in* Saito, S., Underwood, M.B., Kubo, Y., and the Expedition 322 Scientists, *Proceedings of the Integrated Ocean Drilling Program, Expedition 322*: Tokyo, Japan (Integrated Ocean Drilling Program Management International, Inc.), <https://doi.org/10.2204/iodp.proc.322.202.2013>.
- Underwood, M.B., and Guo, J., 2017, Data report: clay mineral assemblages in the upper Shikoku Basin, results from IODP Expedition 333, Sites C0011 and C0012, *in* Henry, P., Kanamatsu, T., Moe, K., and the Expedition 333 Scientists, *Proceedings of the Integrated Ocean Drilling Program, 333*: Tokyo (Integrated Ocean Drilling Program Management International, Inc.), <https://doi.org/10.2204/iodp.proc.333.205.2017>.
- Underwood, M.B., and Pickering, K.T., 1996, Clay-mineral provenance, sediment dispersal patterns, and mudrock diagenesis in the Nankai accretionary prism, southwest Japan: *Clays and Clay Minerals*, v. 44, p. 339–356, <https://doi.org/10.1346/CCMN.1996.0440304>.
- White, R.J., Spinelli, G.A., Mozley, P.S., and Dunbar, N.W., 2011, Importance of volcanic glass alteration to sediment stabilization: Offshore Japan: *Sedimentology*, v. 58, p. 1138–1154, <https://doi.org/10.1111/j.1365-3091.2010.01198.x>.
- Ziegler, C.L., and Murray, R.W., 2007, Geochemical evolution of the central Pacific Ocean over the past 56 Myr: *Paleoceanography*, v. 22, p. 62, <https://doi.org/10.1029/2006PA001321>.
- Ziegler, C.L., Murray, R.W., Hovan, S.A., and Rea, D.K., 2007, Resolving eolian, volcanogenic, and authigenic components in pelagic sediment from the Pacific Ocean: *Earth and Planetary Science Letters*, v. 254, p. 416–432, <https://doi.org/10.1016/j.epsl.2006.11.049>.
- Ziegler, C.L., Murray, R.W., Plank, T., and Hemming, S.R., 2008, Sources of Fe to the equatorial Pacific Ocean from the Holocene to Miocene: *Earth and Planetary Science Letters*, v. 270, p. 258–270, <https://doi.org/10.1016/j.epsl.2008.03.044>.